

**Azobenzene-decorated cellulose nanocrystals as photo-switchable chiral solutes in nematic liquid crystals**

Journal:	<i>Journal of Materials Chemistry C</i>
Manuscript ID	TC-ART-10-2022-004444.R1
Article Type:	Paper
Date Submitted by the Author:	09-Nov-2022
Complete List of Authors:	Sezgin, Baris; Kent State University, Advanced Materials and Liquid Crystal Institute Hegmann, Torsten; Kent State University, Advanced Materials and Liquid Crystal Institute

ARTICLE

Azobenzene-decorated cellulose nanocrystals as photo-switchable chiral solutes in nematic liquid crystals†

Barış Sezgin^{a,b} and Torsten Hegmann^{*b-d}Received 00th October 2022,
Accepted 00th January 2022

DOI: 10.1039/x0xx00000x

In this work, we validate that cellulose nanocrystals (CNCs), surface-functionalized with pro-mesogenic azobenzene pendants, can act as photoswitchable chiral solutes in a nematic liquid crystal (N-LC). Upon UV illumination, the helical pitch and thus the helical twisting power (β_w) can be altered based on the *trans-cis* photoisomerization of the azobenzene pendants. This approach shows that CNCs—biorenewable chiral additives with a commensurate, rod-like shape to the N-LC molecules—can be adapted just like common small molecule organic chiral solutes in LC phases based upon simple surface modifications.

1. Introduction

To examine how the geometry of a chiral object affects chirality transfer to a surrounding medium, earlier approaches focused on the transmission and amplification of chirality from colloidal nanomaterials commonly involving a metal (gold) core differing in shape and overall dimensions.¹ An efficient strategy takes advantage of a suitable reporter medium that allows one to quantify the transmission efficacy of chiral information from a chiral nanoobject to its surrounding.²⁻⁸ Our research has shown that to acquire this knowledge, an induced chiral nematic LC (N*-LC) phase, as a responsive and birefringent medium, can be used quite effectively since the induced helical arrangement of the spatial orientation of the constituent building blocks (molecules, molecular assemblies, or anisometric particles) caused by the addition of chiral nanoscale additives translates to the bulk, thereby facilitating the detection, visualization, and measurement of chirality on length scales easily accessible by optical microscopy between crossed polarizers.⁹ A combination of non-correlated experimental and geometrically derived data revealed how the chirality transfer efficacy depends on the geometry of chiral gold nanoshapes. The underlying mechanism is based on the scalar product of an established pseudoscalar chirality indicator and a scalar geometric shape compatibility factor based on the 2-D isoperimetric ratio for the nanoshape solute and the used N-LC molecules.^{1,10}

Previously studied gold nanoshapes differing in size, shape, and aspect ratio featured surface functionalization by various types of chiral ligands as chiral additives in chirality amplification

studies within an achiral N-LC host serving as the reporter. In that context, all gold nanoshape solutes were comprised of a molecularly and morphologically achiral core capped with a monolayer of 'passive' chiral molecules. In those studies, we established that chiral molecule-decorated rod-like nanoshapes with 2-D isoperimetric quotients matching those of the N-LC host molecules are among the most proficient in their ability to transfer chirality to an N-LC host phase, exhibiting values of the helical twisting power β_w ($\beta_w = (p \cdot c \cdot r)^{-1}$, where p is the helical pitch of the induced N*-LC phase, c the weight fraction of chiral solute (wt.%), and r the enantiomeric purity).¹ Values for β_w and the molar helical twisting power (β_{mol}) were one to two orders of magnitude higher than those of the free organic chiral ligands or some of the strongest common organic chiral additives.¹⁰

Aside from a few exceptions of engineered, helically structured inorganic films¹¹ or inverse helical organic filament networks,¹² nanomaterials with sole or additional core-chirality have only very recently been studied for their ability to transfer chirality.¹³ While potential contributions to the overall chirality by chiral field effects, those generated by a chiral organic ligand shell,¹⁴ or by a chiral adsorption pattern on such plasmonic nanoshapes with high polarizability cannot be overlooked,¹⁵ key questions arising from these prior studies were if and to what extent a potentially chiral core contributes to the overall, highly potent chirality transfer to the surrounding N-LC reporter medium.

To elucidate the role of core chirality, we recently reported on the chirality transfer by nanostructures with an intrinsically chiral core, i.e., cellulose nanocrystals (CNCs) that were further covalently modified with either chiral or achiral molecules.^{16,17} We found that among such CNCs, those functionalized with achiral moieties structurally related to the N-LC, showed better N-LC solubility, and thus serving as efficient chiral inducers with β_w values from $-35 \mu\text{m}^{-1}$ for neat to $-54 \mu\text{m}^{-1}$ for cholesterol-modified CNCs. Here, functionalization with chiral molecules rather than just mesogenic moieties that were structurally alike to the N-LC host only slightly enhanced the efficacy of helical distortion in the host N-LC, indicating the high propensity of CNCs to transfer chirality from an inherently chiral core.¹⁶

^a Department of Chemistry, Süleyman Demirel University, 32260 Isparta, Cunur, Turkey

^b Advanced Materials and Liquid Crystal Institute, Kent State University, Kent (OH) 44242-001 USA; E-mail: thegmann@kent.edu

^c Department of Chemistry and Biochemistry, Kent State University, Kent (OH) 44242-001 USA

^d Materials Science Graduate Program, Kent State University, Kent (OH) 44242-001 USA

† Electronic Supplementary Information (ESI) available: synthesis, characterization data and other experimental details and data; See DOI: 10.1039/x0xx00000x

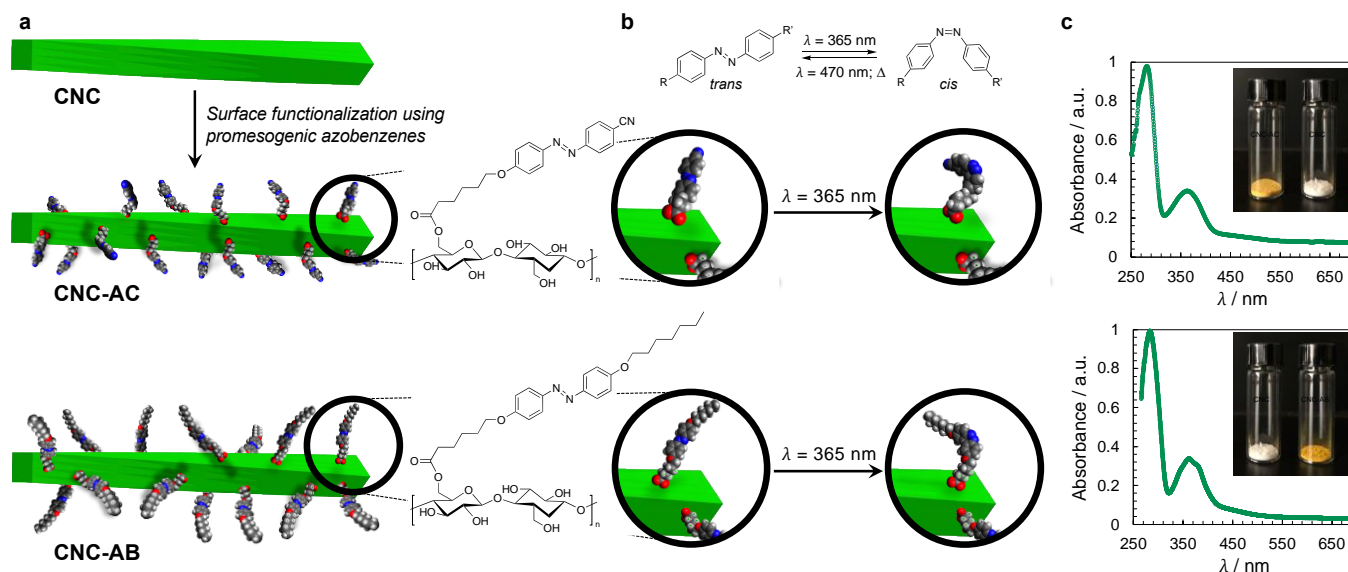


Fig. 1 (a) Concept of CNC surface modification with azobenzene derivatives (AC or AB) and (b) depiction of *trans-cis* photoisomerization of azobenzene moiety – principle (top) and on the surface of the functionalized CNCs. (c) UV-vis spectra of CNC-AC and CNC-AB (DMF, 20 °C) – the major peak at $\lambda \sim 285$ nm is characteristic for acid-treated CNCs,¹⁹ the peak centered at $\lambda \sim 370$ nm for the *trans*-azobenzenes and the small shoulder at $\lambda \sim 480$ nm for the *cis*-azobenzenes (insets show photographs of neat and surface-modified CNCs).

As for the CNC's inherent core chirality, during acid hydrolysis the amorphous regions of the cellulose fibers are cleaved, yielding negatively charged rod-like CNCs of high crystallinity with dimensions ranging from 5 – 20 nm in width and 100 – 500 nm in length.¹⁹ The final nanocrystals are composed of chiral $\beta(1\rightarrow4)$ D-glucose subunits, which render CNCs structurally chiral with a twist in both their internal structure and their outer morphology, either on an individual NC or on the formed bundles level.^{20–30} Their core chirality together with their rod-like shape enables CNCs to self-assemble into left-handed chiral nematic liquid crystal (N*-LC) phases, when dispersed in various solvents (commonly water) or after solvent evaporation.^{31–40} To further enhance the versatility of hydrophobic CNCs as chiral solutes inducing N*-LC phases, the next logical step seemed to decorate CNCs with photoswitchable molecules that allow for 'active' control (switching) of p , thus β_w , by altering the wavelength of light irradiation.^{41–43} Azobenzene derivatives with aliphatic carboxylic acid end groups that allow for CNC surface modification appeared as the most logical initial choice.

The reversible photoisomerization of azobenzene has been and still is used in an extensive array of materials systems and for applications ranging from catalysis^{44–46} over energy harvesting⁴⁷ and actuators⁴⁸ to countless optical applications.^{49,50} The latter presumably receiving the bulk of the attention because of the robust and well-understood *trans-cis* photoisomerization of azobenzene derivatives that can be switched by a combination of light at various wavelengths and temperature.⁵¹

The concept of grafting two structurally purposefully different azobenzene derivatives to CNCs with is schematically shown in Figure 1. CNC-AC features a more polar azobenzene with a terminal cyano-group,⁵² CNC-AB, in contrast, a more apolar terminal aliphatic hydrocarbon chain,⁵³ thus, making this CNC's surface more compatible with the N-LC used in these studies (Felix-2900-03, Figure 2), which is also flanked by two aliphatic side chains.

2. Experimental

2.1 Materials

All reagents used were purchased from Sigma-Aldrich and used without further purification. Cellulose nanocrystals (CNCs) were obtained from CelluForce in the form of the sulphate sodium salt. The two azobenzene pendant molecules in their avid form were prepared out outlined in the Electronic Supplementary Information (ESI; Section S1, Scheme S1 and S2, Figures S1 – S7).

2.2 Methods

¹H NMR spectra were recorded on a Bruker DMX 400 MHz spectrometer. Cross-polarization magic angle spinning (CP-MAS) ¹³C NMR spectra were recorded on a Bruker Avance III (100.6 MHz) 400 NMR spectrometer. 4 mm Zirconia rotors with stirring speeds of 5 kHz were used with 5,000 to 10,000 scans. FT-IR spectra were taken on a Bruker FT-IR Tensor27 system equipped with a Pike miracle ATR (attenuated total reflectance) accessory. Thermogravimetric analysis (TGA) was done using a TGA Q500 (TA Instruments). Differential scanning calorimetry (DSC) experiments were performed using a PerkinElmer Pyris 1 DSC at a heating/cooling rate of 10 °C min⁻¹, reporting data from the first heating and cooling cycle, respectively (temperatures calibrated with In and Zn standards). UV irradiation experiments were carried out at $\lambda = 365$ nm using a UVCureMXLED LED light curing spot gun ($P = 6$ W). Polarized optical microscopy (POM) observations of the induced N*-LC phases were recorded and photographed using an Olympus BX-53 polarizing microscope equipped with a Linkam LTS420E heating/cooling stage. UV-vis data were acquired using an OLIS spectrophotometer (solution data; quartz cuvettes, 1 cm path length). Transmission electron microscopy (TEM) analysis was performed with FEI Tecnai TF20 TEM instrument at an accelerating voltage of 200 kV. XPS spectra were collected with a PHI 5000 Versaprobe XPS using a monochromatic Al K α source (1,486.6 eV). Survey spectra were

collected from 1,100 to 0 eV at a pass energy of 93.90 eV. High resolution C1s spectra were collected at pass energy of 11.75 eV with a scan step of 0.1 eV. Phi MultiPack software was used for data processing. High-resolution XPS spectra were fitted using linear combinations of 70:30 Gauss-Lorentzian functions on Shirley background-subtracted spectra. Binding energy scale was calibrated using aliphatic C1s component, set at 285.0 eV.

3. Results and discussion

3.1 Surface-modified CNC synthesis and characterization

To prepare the azobenzene-functionalized CNCs, we esterified the surface of the CNCs (specifically the primary hydroxyl group at carbon C6) with two promesogenic azobenzene derivatives: one with a terminal cyano group (AC) and one with a terminal aliphatic hydrocarbon chain (AB) as shown in Figure 1. Prior to this step, the sodium sulfonate groups, despite the overall low degree of sulfonation, were converted into sulfonic acid groups to render the CNCs more soluble in organic solvents.

Functionalization of the CNCs with the corresponding carboxylic acids was done using a Steglich esterification (EDC/DMAP) (ESI, Section S1.2).⁵⁴ FT-IR analysis shows that CNCs primary hydroxyl groups were successfully converted, judging from the presence of peaks at about 1700 cm^{-1} and 1600 cm^{-1} , which correspond to the ester C=O stretches and aromatic C=C skeletal vibrations, respectively (ESI, Figure S8).⁴² Moreover, solid-state cross-polarization magic angle spinning (CP-MAS) ^{13}C NMR experiments confirmed that each of the CNCs was indeed functionalized, as seen by the appearance of carbonyl-C peaks at around 175 to 160 ppm, weak aromatic-C peaks between 140 to 120 ppm, and aliphatic carbon signals at around 50 to 10 ppm. The area of the peak corresponding to the C6 amorphous region, labeled as C6 (and small shoulder on the right in Figure S9, ESI), appears to decrease for the functionalized CNC products when compared to the untreated CNCs,¹⁶ and thus indicates the esterification of the C6 hydroxyl groups in the amorphous region.⁵⁵ CP-MAS solid state ^{13}C NMR also demonstrated that the structural crystallinity was preserved.⁵⁶ X-ray photoelectron spectroscopy (XPS) analysis⁵⁷ (ESI, Figure S10 and S11) afforded estimations of the degree of surface functionalization (*DSF*) for the functionalized CNCs, which were calculated to be 0.10 for CNC-AC and 0.17 for CNC-AB (see ESI, Section S2.3).⁵⁸ Thermogravimetric analysis (TGA) of all samples further supported the functionalization by showing altered weight loss curves (ESI, Figure S12).¹⁶ Transmission electron microscopy (TEM) micrographs obtained for the functionalized CNCs corroborate the ^{13}C NMR data by showing that neither crystallinity nor morphology were affected by the surface modifications when compared to the TEM images collected for the unmodified CNCs (ESI, Figure S13).⁵⁹ The average width was determined to be 20 nm and the length varied from about 100 to 150 nm giving an average aspect ratio of 6.25.

3.2 Mixtures of N-LC host doped with CNC solutes

To examine how efficient the surface-modified CNCs can induce a helical distortion of guest molecules of an achiral N-LC host

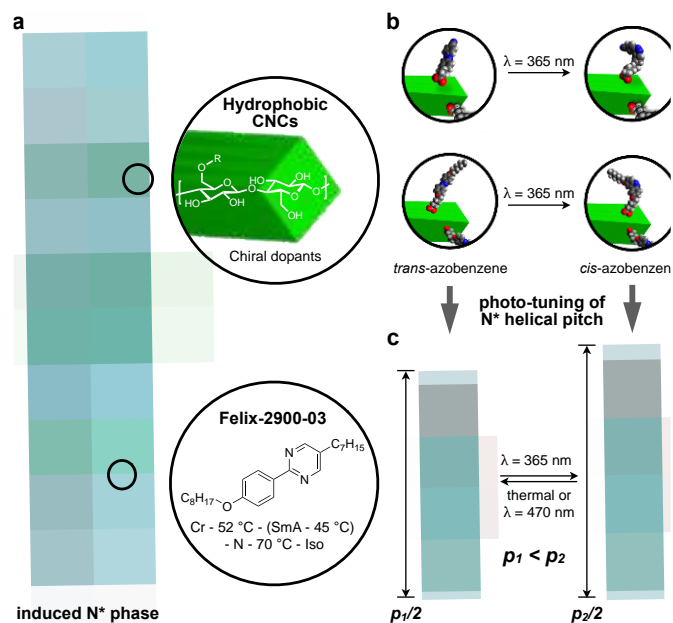


Fig. 2 (a) Schematic representation of the N*-LC phase induced by the addition of minute amounts of the functionalized CNCs in the N-LC host, Felix-2300-03. (b) The *trans-cis* photoisomerization of the azobenzene pendants (AC or AB) induced by illumination with UV light (at $\lambda = 365 \text{ nm}$) to prompt (c) an increase in the helical pitch (p) when the azobenzenes are in their cis configuration.

medium, we prepared and examined binary mixtures at various concentrations of the functionalized CNCs in the N-LC phase of Felix-2900-03. Minute amounts of the chiral CNC additives were added at a temperature just above the isotropic-nematic phase transition ($T_{\text{iso-N}}$) of the N-LC to formulate mixtures, ranging from 0.05 to 2.0 wt.% CNCs, which were rigorously sonicated and then slowly cooled down until a phase transition to the induced N*-LC was observed. The textural characteristics of the induced N*-LC phase would thereby evidence chirality transfer from the CNCs chiral core to the achiral N-LC bulk.

Polarized optical microscopy (POM) studies of the CNC-doped samples prepared between untreated glass slides shows the formation of the characteristic fingerprint textures, resulting from the induction of an N*-LC phase with values of p ranging from about 6 – 8 μm at 0.05 wt.% and 3 – 4 μm at 0.2 wt.% prior to illumination with 365 nm UV light (Figure 3). As expected, decreases with an increasing concentration of either CNC, but lower values are observed throughout each series for CNC-AB featuring azobenzene pendants that more closely resemble the N-LC host (either one is flanked by two aliphatic side chains). Noteworthy, neither of the two azobenzene-decorated CNCs reported here is as effective with respect to inducing a tighter pitch (leading to higher values for β_w) as the previously tested CNCs that were decorated with mesogenic pendants that either mimicked the host N-LC or were chiral nematic LCs as such as the cholesterol-decorated CNCs.¹⁶ However, illumination with UV light at $\lambda = 365 \text{ nm}$ resulted in the expected pitch increase of the induced N*-LC phase⁶⁰⁻⁶⁷ for concentrations of each of the CNCs not exceeding 0.15 wt.% (Figure 4). A further increase of the CNC concentration to 0.2 wt.% for both CNC-AC and CNC-AB led to an increase in p after UV illumination at $\lambda = 365 \text{ nm}$ (Figure 4) that is surely linked to the increasing incompatibility

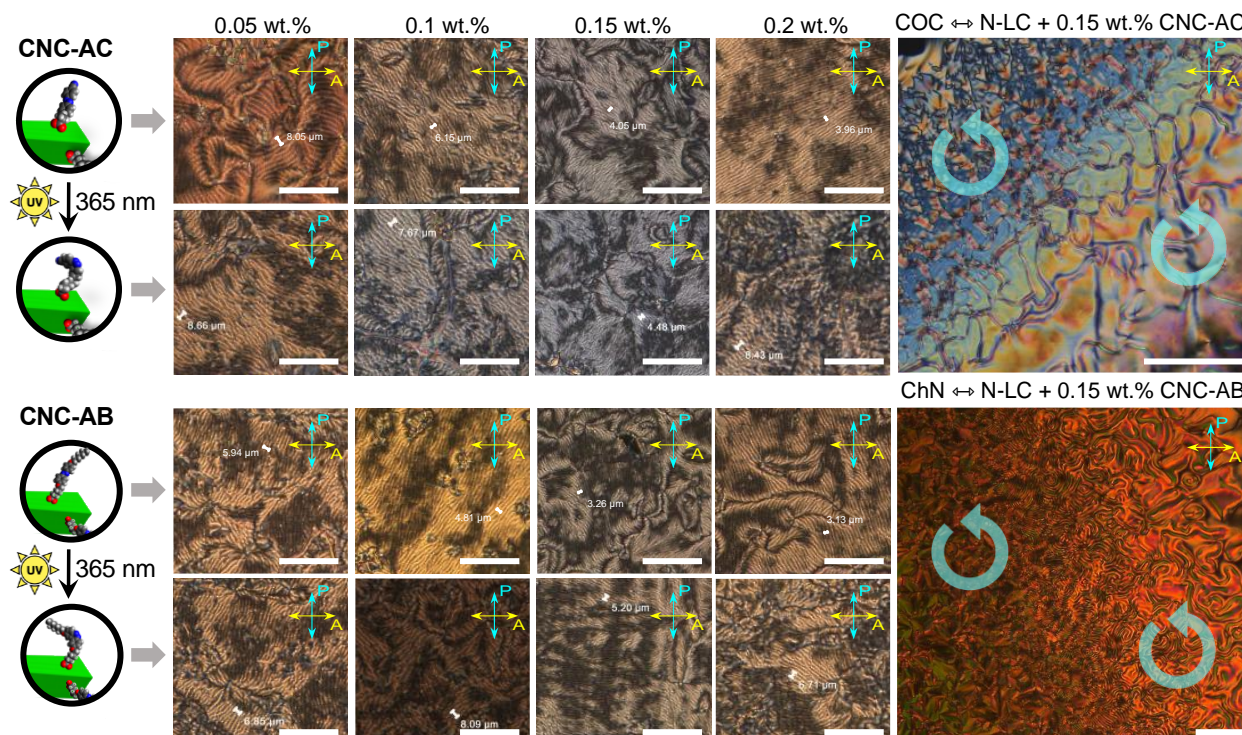


Fig. 3 POM photomicrographs (crossed polarizer, P, and analyzer, A) taken on cooling from the isotropic liquid phase at $T = 45\text{ }^{\circ}\text{C}$, showing the fingerprint textures obtained from samples prepared between two untreated glass slides of Felix-2900-03 doped with CNC-AC or CNC-AB before and after illumination with UV light at a wavelength of $\lambda = 365\text{ nm}$ at concentrations of the CNCs ranging from 0.05 to 0.2 wt.% as indicated above each column of images. Images on the right of each set show the contact preparations with cholesteryl oleyl carbonate (COC) for CNC-AC (taken at $T = 45\text{ }^{\circ}\text{C}$ on cooling) or cholesteryl nonanoate (ChN) for CNC-AB (taken at $T = 65\text{ }^{\circ}\text{C}$ on cooling), and in each case no discontinuation was seen in contact with the two known left-handed N^* -LCs (handedness is indicated by light blue circular arrows). Scale bars = $50\text{ }\mu\text{m}$.

(lower miscibility)⁵ of the CNCs with the ensuing *cis*-configuration (Figure 5) of the two azobenzene pendants on the CNC surfaces in the N-LC as reported previously in numerous studies.⁶⁰⁻⁶⁷

The handedness of the induced N^* -LC phase was analyzed using contact preparations with cholesteryl oleyl carbonate (COC) or cholesterol nonanoate (ChN), each known to form left-handed N^* -LC phases.^{68,69} Since no discontinuation (i.e., no achiral N-LC phase) was seen in the contact zone with COC (ChN), this reveals that the CNCs induced a left-handed N^* -LC phase just like the previous CNC chiral solutes in this N-LC host¹⁶ or their native handedness in aqueous suspension.³⁴ The values for β_w derived from the measured ρ data are comparatively lower than for the previous mesogen-crafted CNCs,¹⁶ here $\beta_w = -2.14\text{ }\mu\text{m}^{-1}$ for CNC-AB and $-1.70\text{ }\mu\text{m}^{-1}$ for CNC-AC prior to UV exposure and $-1.39\text{ }\mu\text{m}^{-1}$ and $-1.50\text{ }\mu\text{m}^{-1}$ (“-” meaning left-handed) after UV illumination (ESI, Figure S14), which we attribute to a more limited compatibility of the azobenzene moieties with the used N-LC. In fact, both azobenzene-decorated CNCs described here appear less soluble in Felix-2900-03, which we relate to two factors: (1) Neither of the azobenzene pendants is liquid crystalline at the temperature range of the studied N-LC host. Only AC is monotropic nematic with a phase sequence of Iso 202 N 162 Cr on cooling (with some degree of decomposition after the first heating);⁵² AB, however, is non-mesogenic.⁵³ (2) Small fractions of the azobenzene pendants are already in the *cis*-configuration even before UV illumination, which can be seen in the UV-vis spectra shown in Figure 1c. Deconvolution of the peaks in the UV spectra prior to UV illumination indicates that

for CNC-AC 27% of the AC units and for CNC-AB 26% of the AB units, respectively, are in the *cis* configuration (ESI, Figure S15).

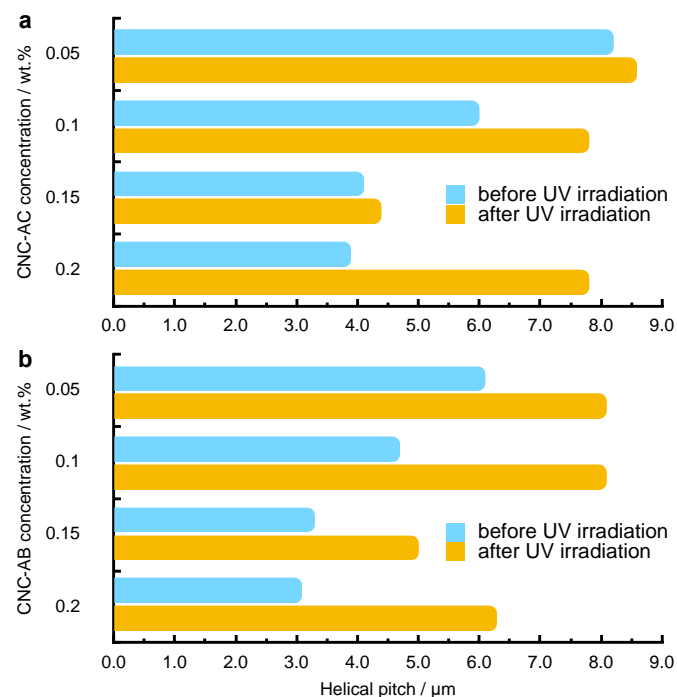


Fig. 4 Plots of the measured helical pitch (ρ) at $5\text{ }^{\circ}\text{C}$ above the N-SmA phase transition on cooling from the isotropic liquid phase versus the concentration of: (a) CNC-AC and (b) CNC-AB. Light blue upper data bars in each plot and for each concentration are samples prior to illumination with UV light, yellow lower bars after UV illumination.

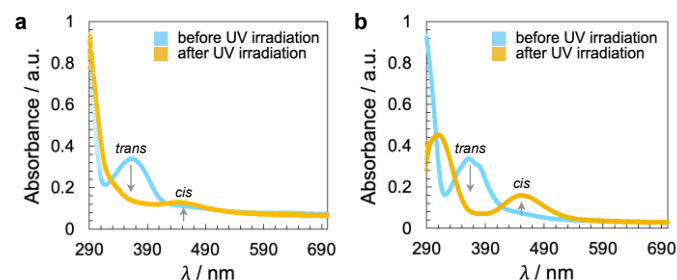


Fig. 5 UV-vis spectra of the CNCs in DMF (20 °C) before and after illumination with UV light at $\lambda = 365$ nm for a time period of $t = 10$ s: (a) CNC-AC and (b) CNC-AB. Longer exposure, up to $t = 60$ s, did not lead to a discernible change in the spectra, and thus, all azobenzene pendants are already in the *cis* configuration in solution after a $t = 10$ s exposure to UV light (ESI, Figure S16).

The change in p under $\lambda = 365$ nm illumination is reasonably fast (seconds), but the thermal *cis*-to-*trans* back relaxation of the azobenzene units is significantly slower (several tens of minutes or more). However, by heating the sample back to the isotropic liquid phase (i.e., to higher temperatures), samples recover the tighter pitch values seen prior to UV illumination (ESI, Fig. S17).

4. Conclusions

CNCs may not be ideal chiral additive for some applications, but their origin from a wide range of renewable resources⁷⁰ coupled with facile opportunities for surface functionalization renders them a new opportunity in the realm of chiral solutes. We here verified that surface modification with an active photoswitch in the form of azobenzene pendants leads to CNCs as chiral solutes that can induce N*-LC phases with a phototunable helical pitch. Predictive, and following the earlier trend,¹⁶ CNC-AB, which is decorated with azobenzene pendants that are structurally more alike to the N-LC host shows both higher values for β_w as well as more effective photomodulation of p as verified by comparing the values of $\Delta\beta_w$ ($0.75 \mu\text{m}^{-1}$ for CNC-AB and $0.20 \mu\text{m}^{-1}$ for CNC-AC, respectively). This may be further exacerbated by the higher *DSF* value for CNC-AB in comparison to CNC-AC. In CNC-AC, only one of every ten D-glucose subunits is functionalized with an AC pendant, for CNC-AB this rises to one AB pendant in almost every six D-glucose subunits, thus, rendering CNC-AB not only more compatible (structurally) but also more miscible.

Further opportunities to optimize this system are available via the use of more effective (higher β_w), better soluble (miscible), room temperature mesogenic and photoswitchable pendant molecules^{61,65} or by selecting (preparing) CNC aspect ratios⁷¹ that would provide an improved match to N-LC host molecules aspect ratio based on our earlier work on matching the 2-D isoperimetric ratio of nanoscale chiral solutes in N-LCs,¹ which is work that is currently ongoing in our laboratory. Ultimately, photoresponsive (photoswitchable) CNCs may find applications requiring stimuli-responsive^{48,72} and smart nanoarchitectonic⁷³⁻⁷⁷ materials for chiral photonics,⁷⁸⁻⁸⁰ soft actuators, and other adaptive materials⁸¹ based on their renewable nature and high versatility.

Author Contributions

B.S. performed the synthesis and characterization of the materials, sample preparation, and all measurements. B.S. and T.H. analyzed the data and co-wrote the manuscript. T.H. directed the study.

Conflicts of interest

There are no conflicts to declare.

Acknowledgements

This work was financially supported by The Scientific and Technological Research Council of Turkey (TUBITAK) - 2214-A - International Research Fellowship Program (1059B142100482, B.S.), the U.S. National Science Foundation (NSF, DMR-1904091; T.H.), and the Ohio Third Frontier (OTF) program for Ohio Research Scholars "Research Cluster on Surfaces in Advanced Materials", which also supports the Materials Characterization and Imaging Facility at the Advanced Materials and Liquid Crystal Institute (AMLCI) at Kent State University, where current TEM data were acquired. We thank the Swagelok Center for Surface Analysis of Materials at Case Western Reserve University and Dr. T. K. J. Kim for access to and assistance with the XPS experiments and data analysis. Finally, we acknowledge the help of Dr. M. Gangoda for CP-MAS ¹³C NMR spectroscopy experiments.

References

- 1 A. Nemati, L. Querciagrossa, C. Callison, S. Shadpour, D. P. N. Gonçalves, T. Mori, X. Cui, R. Ai, J. Wang, C. Zannoni, T. Hegmann, *Sci. Adv.* 2022, **8**, eabl4385
- 2 A. Sharma, T. Mori, H.-C. Lee, M. Worden, E. Bidwell, T. Hegmann, *ACS Nano* 2014, **8**, 11966-11976.
- 3 T. Mori, A. Sharma, T. Hegmann, *ACS Nano* 2016, **10**, 1552-1564.
- 4 R. K. Shukla, A. Sharma, T. Mori, T. Hegmann, W. Haase, *Liq. Cryst.* 2016, **43**, 695-703.
- 5 A. Nemati, S. Shadpour, L. Querciagrossa, L. Li, T. Mori, M. Gao, C. Zannoni, T. Hegmann, *Nat. Commun.* 2018, **9**, 3908.
- 6 S. Shadpour, J. P. Vanegas, A. Nemati, T. Hegmann, *ACS Omega* 2019, **4**, 1662-1668.
- 7 A. Nemati, S. Shadpour, L. Querciagrossa, T. Mori, C. Zannoni, T. Hegmann, *ACS Nano* 2019, **13**, 10312-10326.
- 8 A. Poryvai, M. Šmahel, M. Švecová, A. Nemati, S. Shadpour, P. Ulbrich, T. Ogolla, J. Liu, V. Novotná, M. Veverka, J. Vejpravová, T. Hegmann, M. Kohout, *ACS Nano* 2022, **16**, 11833-11841.
- 9 D. P. N. Gonçalves, M. E. Prévôt Ş. Üstünel, T. Ogolla, A. Nemati, S. Shadpour, T. Hegmann, *Liq. Cryst. Rev.* 2021, **9**, 1-34.
- 10 A. Sharma, T. Mori, A. Nemati, D. P. N. Gonçalves, L. Querciagrossa, C. Zannoni, T. Hegmann, *Mater. Adv.* 2022, **3**, 3346-3354.
- 11 K. Robbie, D. J. Broer, M. J. Brett, *Nature* 1999, **399**, 764-766.
- 12 J.-J. Lee, B.-C. Kim, H.-J. Choi, S. Bae, F. Araoka, S.-W. Choi, *ACS Nano* 2020, **14**, 5243-5250.
- 13 X. Zhang, Y. Xu, C. Valenzuela, X. Zhang, L. Wang, W. Feng, Q. Li, *Light: Sci. & Appl.* 2022, **11**, 223.
- 14 S. O. Pour, L. Rocks, K. Faulds, D. Graham, V. Parčhaňský, P. Bouř, E. W. Blanch, *Nat. Chem.* 2015, **7**, 591-596.

- 15 W. Ma, L. Xu, A. F. de Moura, X. Wu, H. Kuang, C. Xu, N. A. Kotov, *Chem. Rev.* 2017, **117**, 8041-8093.
- 16 D. P. N. Gonçalves, T. Hegmann, *Angew. Chem. Int. Edit.* 2021, **60**, 17344-17349.
- 17 D. P. N. Gonçalves, T. Ogolla, T. Hegmann, *ChemPhysChem* 2022, in press, DOI:10.1002/cphc.202200685.
- 18 S. K. Shukla, G. C. Dubey, A. Tiwari, A. Bharadvaja, *Adv. Mater. Lett.* 2013, **4**, 714-719.
- 19 T. Abitbol, A. Rivkin, Y. Cao, Y. Nevo, E. Abraham, T. Ben-Shalom, S. Lapidot, O. Shoseyov, *Curr. Opin. Biotechnol.* 2016, **39**, 76-88.
- 20 W. J. Orts, L. Godbout, R. H. Marchessault, J.-F. Revol, *Macromolecules* 1998, **31**, 5717-5725.
- 21 J. Araki, S. Kuga, *Langmuir* 2001, **17**, 4493-4496.
- 22 S. Elazzouzi-Hafraoui, Y. Nishiyama, J.-L. Putaux, F. F. Dubreuil, C. Rochas, *Biomacromolecules* 2008, **9**, 57-65.
- 23 I. Usov, G. Nyström, J. Adamclik, S. Handschin, C. Schütz, A. Fall, L. Bergström, R. Mezzenga, *Nat. Commun.* 2015, **6**, 7564-7575.
- 24 K. Conley, L. Godbout, M. A. Whitehead, T. G. M. Van DE Ven, *Carbohydr. Polym.* 2016, **135**, 285-299.
- 25 Y. Ogawa, *Nanoscale* 2019, **11**, 21767-21774.
- 26 G. Delepierre, S. Eyley, W. Thielemans, C. Weder, E. D. Cranston, J. O. Zoppe, *Nanoscale* 2020, **12**, 17480-17493.
- 27 S. Gim, G. Fittolani, Y. Nishiyama, P. H. Seeberger, Y. Ogawa, M. Delbianco, *Angew. Chem. Int. Ed.* 2020, **59**, 22577-22583.
- 28 K. Uetani, T. Uto, N. Suzuki, *Sci. Rep.* 2021, **11**, 790.
- 29 T. Willhammar, K. Daicho, D. N. Johnstone, K. Kobayashi, Y. Liu, P. A. Midgley, L. Bergström, T. Saito, *ACS Nano* 2021, **15**, 2730-2737.
- 30 T. G. Parton, R. M. Parker, G. T. van de Kerkhof, A. Narkevicius, J. S. Haataja, B. Frka-Petesic, S. Vignolini, *Nat. Commun.* 2022, **13**, 2657.
- 31 Y. Habibi, L. A. Lucia, O. J. Rojas, *Chem. Rev.* 2010, **110**, 3479-3500.
- 32 J. Majoinen, E. Kontturi, O. Ikkala, D. G. Gray, *Cellulose* 2012, **19**, 1599-1605.
- 33 J. A. Kelly, A. M. Shukaliak, C. C. Y. Cheung, K. E. Shopsowitz, W. Y. Hamad, M. J. MacLachlan, *Angew. Chem. Int. Ed.* 2013, **52**, 8912-8916.
- 34 J. P. F. Lagerwall, C. Schütz, M. Salajkova, J. Noh, J. H. Park, G. Scalia, L. Bergström, *NPG Asia* 2014, **6**, e80.
- 35 P.-X. Wang, W. Y. Hamad, M. J. MacLachlan, *Nat. Commun.* 2016, **7**, 11515.
- 36 Y. Li, J. Jun-Yan Suen, E. Prince, E. M. Larin, A. Klinkova, H. Thérien-Aubin, S. Zhu, B. Yang, A. S. Helmy, O. D. Lavrentovich, E. Kumacheva, *Nat. Commun.* 2016, **7**, 12520.
- 37 O. Liu, I. I. Smalyukh, *Sci. Adv.* 2017, **3**, e1700981.
- 38 B. Vollick, P.-Y. Kuo, H. Thérien-Aubin, N. Yan, E. Kumacheva, *Chem. Mater.* 2017, **29**, 789-795.
- 39 O. Kose, A. Tran, L. Lewis, W. Y. Hamad, M. J. MacLachlan, *Nat. Commun.* 2019, **10**, 510.
- 40 R. Kádár, S. Spirk, T. Nypelö, *ACS Nano* 2021, **15**, 7931-7945.
- 41 X. Liu, M. Li, X. Zheng, E. Retulainen, S. Fu, *Materials* 2018, **11**, 1725.
- 42 I. Otsuka, C. J. Barrett, *Cellulose* 2019, **26**, 6903-6915.
- 43 Z. Xu, S. Peng, G. Zhou, X. Xu, *J. Compos. Sci.* 2020, **4**, 186.
- 44 M. V. Peters, R. S. Stoll, A. Kühn, S. Hecht, *Angew. Chem. Int. Ed.* 2008, **47**, 5968-5972.
- 45 T. Imahori, R. Yamaguchi, S. Kurihara, *Chem. - Eur. J.* 2012, **18**, 10802-10807.
- 46 L. Osorio-Planes, C. Rodríguez-Escrich, M. A. Pericàs, *Org. Lett.* 2014, **16**, 1704-1707.
- 47 B. Zhang, Y. Feng, W. Feng, *Nano-Micro Lett.* 2022, **14**, 138.
- 48 For a recent review, see: X. Pang, J. Lv, L. Qin, Y. Yu, *Adv. Mater.* 2019, **31**, 1904224.
- 49 Z. Chu, Y. Han, T. Bian, S. De, P. Král, R. Klajn, *J. Am. Chem. Soc.* 2019, **141**, 1949-1960.
- 50 Q. M. Zhang, X. Li, M. R. Islam, M. Wei, M. J. Serpe, *J. Mater. Chem. C* 2014, **2**, 6961-6965.
- 51 M. Quick, A. L. Dobryakov, M. Gerecke, C. Richter, F. Berndt, I. N. Ioffe, A. A. Granovsky, R. Mahrwald, N. P. Ernsting, S. A. Kovalenko, *J. Phys. Chem. B* 2014, **118**, 8756-8771.
- 52 G. Mao, J. Wang, S. R. Clingman, C. K. Ober, J. T. Chen, E. L. Thomas, *Macromolecules* 1997, **30**, 2556-2567.
- 53 M. Matsumoto, K. Tanaka, R. Azumi, Y. Kondo, N. Yoshino, *Langmuir* 2004, **20**, 8728-8734.
- 54 Y. Wang, X. Wang, Y. Xie, K. Zhang, *Cellulose* 2018, **25**, 3703-3731.
- 55 H. Kono, S. Yunoki, T. Shikano, M. Fujiwara, T. Erata, M. Takai, *J. Am. Chem. Soc.* 2002, **124**, 7506-7511.
- 56 A. Brinkmann, M. Chen, M. Couillard, Z. J. Jakubek, T. Leng, L. J. Johnston, *Langmuir* 2016, **32**, 6105-6114.
- 57 G. Rodionova, M. Lenes, Ø. Eriksen, Ø. Gregersen, *Cellulose* 2011, **18**, 127-134.
- 58 Among the many reports for surface functionalization of CNCs by esterification, the degree of surface functionalization, *DSF*, is typically ≤ 1 and can be as low as 0.06; see: S. Eyley, W. Thielemans, *Nanoscale* 2014, **6**, 7764-7779.
- 59 J. Meija, M. Bushell, M. Couillard, S. Beck, J. Bonevich, K. Cui, J. Foster, J. Will, D. Fox, W. Cho, M. Heidelmann, B. C. Park, Y. C. Park, L. Ren, L. Xu, A. B. Stefaniak, A. K. Knepp, R. Theissmann, H. Purwin, Z. Wang, N. de Val, L. J. Johnston, *Anal. Chem.* 2020, **92**, 13434-13442.
- 60 Q. Li, L. Green, N. Venkataraman, I. Shiyonovskaya, A. Khan, A. Urbas, J. W. Doane, *J. Am. Chem. Soc.* 2007, **129**, 12908-12909.
- 61 Y. Wang, Q. Li, *Adv. Mater.* 2012, **24**, 1926-1945.
- 62 Y. Kim, N. Tamaoki, *J. Mater. Chem. C* 2014, **2**, 9258-9264.
- 63 A. Varanytsia, L.-C. Chien, *Opt. Lett.* 2015, **40**, 4392-4395.
- 64 Y. Kim, N. Tamaoki, *ACS Appl. Mater. Interfaces* 2016, **8**, 4918-4926.
- 65 H. K. Bisoyi, Q. Li, *Chem. Rev.* 2016, **116**, 15089-15166.
- 66 Y. Kim, N. Tamaoki, *ChemPhotoChem* 2019, **3**, 284-303.
- 67 Y. Kim, N. N. Mafy, S. Maisonnette, C. Lin, N. Tamaoki, J. Xie, *ACS Appl. Mater. Interfaces* 2020, **12**, 52146-52155.
- 68 T. Mori, M. Kyotani, K. Akagi, *Chem. Sci.* 2011, **2**, 1389-1395.
- 69 K. Akagi, T. Mori, *Chem. Rec.* 2008, **8**, 395-406.
- 70 J. Gong, J. Li, J. Xu, Z. Xiang, L. Mo, *RSC Adv.* 2017, **7**, 33486-33493.
- 71 X. Wang, C. H. Chang, J. Jiang, Q. Liu, Y.-P. Liao, L. Lu, L. Li, X. Liu, J. Kim, A. Ahmed, A. E. Nel, T. Xia, *Small* 2019, **15**, 1901642.
- 72 R. Nasser, C. P. Deutschman, L. Han, M. A. Pope, K. C. Tam, *Mater. Today Adv.* 2020, **5**, 100055.
- 73 K. Ariga, *Nanoscale Horizons* 2021, **6**, 364-378.
- 74 P. Lv, X. Lu, L. Wang, W. Feng, *Adv. Funct. Mater.* 2021, **31**, 2104991.
- 75 J. Ma, Y. Yang, C. Valenzuela, X. Zhang, L. Wang, W. Feng, *Angew. Chem. Int. Ed.* 2022, **61**, e202116219.
- 76 L. Wang, A. M. Urbas, Q. Li, *Adv. Mater.* 2020, **32**, 1801335.
- 77 X. Zhang, Y. Yang, P. Xue, C. Valenzuela, Y. Chen, X. Yang, L. Wang, W. Feng, *Angew. Chem. Int. Ed.* 2022, **61**, e202211030.
- 78 L. Wang, Q. Li, *Chem. Soc. Rev.* 2018, **47**, 1044-1097.
- 79 L. Dong, Y. Feng, L. Wang, W. Feng, *Chem. Soc. Rev.* 2018, **47**, 7339-7368.
- 80 F. Zhai, Y. Feng, K. Zhou, L. Wang, Z. Zheng, W. Feng, *J. Mater. Chem. C* 2019, **7**, 2146-2171.
- 81 J. Yang, X. Zhang, X. Zhang, L. Wang, W. Feng, Q. Li, *Adv. Mater.* 2021, **33**, 2004754.

